8-31-2021

Recurrent Pattern of Extreme Fire Weather in California

Rackhun Son
Gwangju Institute of Science and Technology

S-Y Simon Wang
Utah State University

Seung Hee Kim
Chapman University, sekim@chapman.edu

Hyungjun Kim
The University of Tokyo

Jee-Hoon Jeong
Chonnam National University

See next page for additional authors

Recommended Citation

Rackhun Son *et al* 2021 *Environ. Res. Lett.* **16** 094031
https://doi.org/10.1088/1748-9326/ac1f44

Recurrent Pattern of Extreme Fire Weather in California

Authors

Rackhun Son, S-Y Simon Wang, Seung Hee Kim, Hyungjun Kim, Jee-Hoon Jeong, and Jin-Ho Yoon

ENVIRONMENTAL RESEARCH
LETTERS

LETTER • **OPEN ACCESS**

Recurrent pattern of extreme fire weather in California

To cite this article: Rackhun Son *et al* 2021 *Environ. Res. Lett.* **16** 094031

IOP Publishing Environ. Res. Lett. 16 (2021) 094031 https://doi.org/10.1088/1748-9326/ac1f44

ENVIRONMENTAL RESEARCH
LETTERS

OPEN ACCESS

RECEIVED
15 June 2021

REVISED
26 July 2021

ACCEPTED FOR PUBLICATION
19 August 2021

PUBLISHED
31 August 2021

LETTER

Recurrent pattern of extreme fire weather in California

Rackhun Son[1], S-Y Simon Wang[2,8], Seung Hee Kim[3], Hyungjun Kim[4,6,7], Jee-Hoon Jeong[5] and Jin-Ho Yoon[1,*]

[1] School of Earth Sciences and Environmental Engineering, Gwangju Institute of Science and Technology, Gwangju, Korea
[2] Department of Plants, Soils, and Climate, Utah State University, Logan, UT, United States of America
[3] Center of Excellence in Earth Systems Modeling and Observations, Chapman University, Orange, CA, United States of America
[4] Institute of Industrial Science, The University of Tokyo, Tokyo, Japan
[5] Faculty of Earth and Environmental Sciences, Chonnam National University, Gwangju, Korea
[6] Moon Soul Graduate School of Future Strategy, Korea Advanced Institute of Science and Technology, Daejeon, Korea
[7] Department of Civil and Environmental Engineering, Korea Advanced Institute of Science and Technology, Daejeon, Korea
[8] International Bachelor Program of Agribusiness, National Chung Hsing University, Taichung, Taiwan
* Author to whom any correspondence should be addressed.

E-mail: yjinho@gist.ac.kr

Keywords: fire weather, variability, California

Supplementary material for this article is available online

Abstract

Historical wildfire events in California have shown a tendency to occur every five to seven years with a rapidly increasing tendency in recent decades. This oscillation is evident in multiple historical climate records, some more than a century long, and appears to be continuing. Analysis shows that this 5–7 year oscillation is linked to a sequence of anomalous large-scale climate patterns with an eastward propagation in both the ocean and atmosphere. While warmer temperature emerges from the northern central Pacific to the west coast of California, La Niña pattern develops simultaneously, implying that the lifecycle of the El Niño-Southern Oscillation that takes multiple years to form could be a trigger. The evolving patterns of the Pacific-to-North America atmospheric teleconnection suggest the role of tropical and subtropical forcing embedded in this lifecycle. These results highlight the semi-cyclical hydrological behavior as a climate driver for wildfire variability in California.

1. Introduction

According to the California Department of Forestry and Fire Protection (CAL FIRE), most of the top 20 fires in California occurred since the year 2000 (bars in figure 1(a)). On top of that, the complex fire which occurred on August 2020 broke records as one of the most severe fires in California (CNN[6], 6 October 2020), and authorities are now concerned of upcoming exceptional danger of drought and fire in the US west (NOAA[7], 29 April 2021). These series of catastrophic events urge to identify sequential pattern of fire related climate phenomena to restrict fire damage ahead. Upon examining the burned area and number of fire statistics from the Monitoring Trends in Burning Severity (MTBS, lines in figure 1(a)), it was observed that significant wildfire damages in California tend to occur every five to seven years since the late 20th century (grey columns in figure 1(a)), a feature that could be periodic in nature that is studided herein.

Fire is intimately tied to ecosystems through interactions with vegetation and climate. As an ecosystem process, fire regulates spatial distribution and composition of vegetation (McLauchlan *et al* 2020). Vegetation structure, in terms of fuel source, influences fire regimes by selecting particular traits and species to survive within a given fire regime (Rogers *et al* 2015) and therefore fire probability and severity. Climate also has a major influence on fire regimes across diverse scales ranging from short-term fire weather to seasonal and decadal variability. Particularly in California, where the wet-dry season is distinct, climate variability plays a crucial role in fire weather condition. Considering this interactive relationship, the apparent oscillation in California raises a possible physical coupling between fire, vegetation and climate.

[6] https://edition.cnn.com/2020/10/06/us/gigafire-california-august-complex-trnd/index.html.
[7] www.ncei.noaa.gov/news/us-drought-monitor-update-april-27-2021.

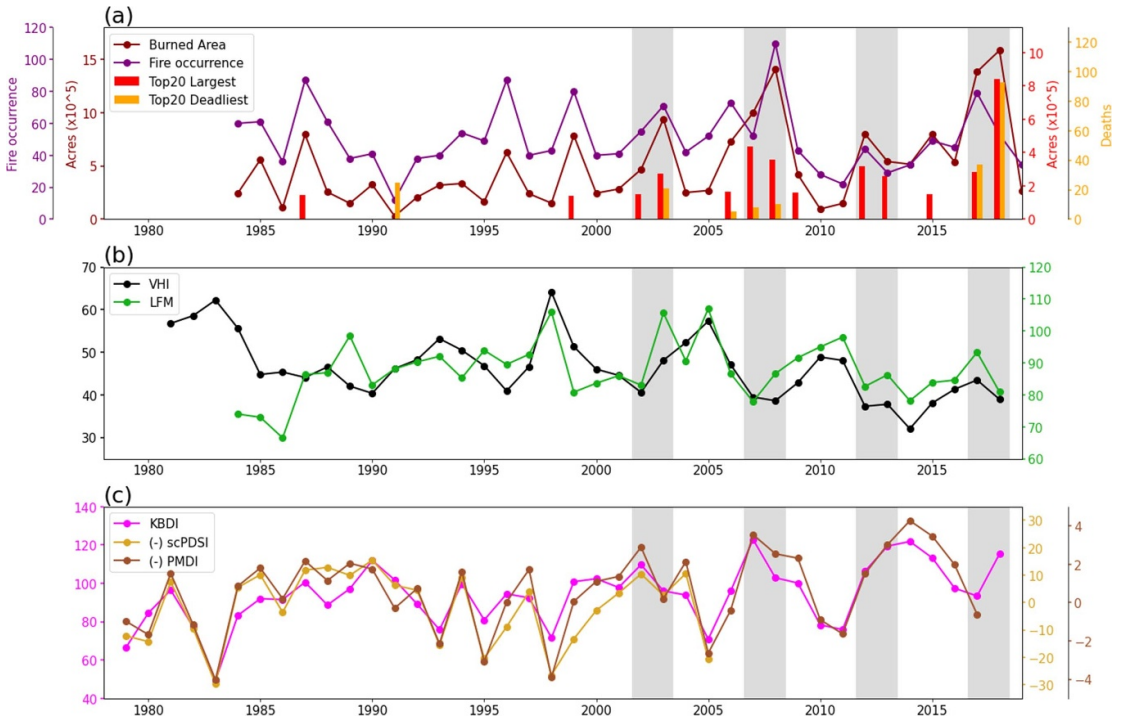

Figure 1. Time-series of wildfire related indices in California. (a) Annual mean of burned area and number of fire occurrence (MTBS, lines), and damage statistics of top 20 the largest and the deadliest fires in California history (CAL FIRE, bars), (b) VHI and LFM, (c) KBDI, scPDSI and PMDI (only PMDI is for June–July–August). All indices are averaged only for California region. The grey columns are marked for the years with catastrophic fire damages at 5–6 year intervals after the year 2000.

Due to the documented enhancement in fire weather associated with the increasing temperature (Jolly *et al* 2015), historical observation and climate model experiments have indicated an aggravated risk in widespread fires under climate change (Abatzoglou *et al* 2019; Liu *et al* 2010, Yoon *et al* 2015). Natural climate variability that modulates California's water cycle extremes strongly modulates its fire potential and occurrence (Yoon *et al* 2015). The underlying climate variations in California and their link with the Pacific Ocean have been widely analyzed, and such natural variability, with an important contribution from the evolution cycle of the El Niño-Southern Oscillation (ENSO), affects California's precipitation (Rajagopalan and Lall 1998), vegetation carbon uptake (Keeling *et al* 1995) and groundwater (Wang *et al* 2015). Here, we present observation-based climate diagnostics of the puzzling quasi-periodic variation of California's fire occurrences (figure 1(a)) and its connection with the recent drought cycle.

2. Data and methods

2.1. Meteorological data

The Vegetation Health Index (VHI) (Kogan 1995) is a combined estimation of moisture and thermal condition using the Normalized Difference Vegetation Index (NDVI) and the brightness temperatures provided from Blended Vegetation Health Products. The live fuel moisture (LFM) (Pollet and Brown 2007), which is a ratio of weight between the fresh and dry vegetation, represents the amount of water content and the flammability of vegetation (Dimitrakopoulos and Papaioannou 2001). The LFM database is *in-situ* measured and maintained by the U.S Forest Service—Wildland Fire Assessment System. For the risks of wildfire and drought, we use the Keetch-Byram Drought Index (KBDI) (Keetch and Byram 1968) provided from ERA5 (Hersbach *et al* 2020) (0.25° × 0.25°, 1979–present) and self-calibrating Palmer Drought Severity Index (scPDSI) (Wells *et al* 2004) from NCAR (Dai *et al* 2004) (2.5° × 2.5°, 1950–2014). To access long-term drought data, summer averaged Palmer Modified Drought Index (PMDI) (Palmer 1965, Karl 1986, Heddinghaus and Sabol 1991), reconstructed by tree-ring, from Living Blended Drought Atlas (Cook *et al* 2010) is also used for 1500–2017. Climatic Research Unit (CRU) also provides long-term land domain temperature and precipitation (0.5° × 0.5°) for time since year 1901 (Harris *et al* 2020). Also, we use a precipitation dataset from the Japanese 55 year Reanalysis (Kobayashi *et al* 2015) (JRA55, 1.25° × 1.25°, 1958–present) to look at the ocean domain. For other climate factors, sea surface temperature (SST) is from the Extended Reconstructed SST version 5 (Huang *et al* 2017) (ERSSTv5, 2.0° × 2.0°, 1854–present), and geopotential height is from JRA55. The soil moisture

content at 100 cm depth is compared with three different land surface models from the North American Land Data Assimilation System (NLDAS-2): Mosaic (Koster and Suarez 1992), Noah (Chen *et al* 1996) and VIC (Liang *et al* 1994).

2.2. Multiple-taper spectrum estimation method with singular value decomposition (MTM-SVD) analysis

An important part of the proposed analysis is to identify the shared frequency in the coupling between fire, vegetation, and climate. The frequency domain SVD provides coherent climate structure across a multivariate dataset. Before a set of climate variable series are decomposed into orthogonal modes, each component is standardized by removing climatological seasonal cycle and dividing by the standard deviation. The constituent series are transformed the spectrum domain using multitaper spectral analysis (Thomson 1982, Park *et al* 1987, Mann and Lees 1996). With these series x, the orthogonal sequences of K data tapers are calculated at each frequency f,

$$Y_k^{(m)}(f) = \sum_{t=1}^{N} w_t^{(k)} x_n e^{i2\pi ft\Delta t}, \tag{1}$$

where Δt is the sampling interval (1 month), M is the number of grid points and N is the time dimension. $\left\{w_t^{(k)}\right\}_{t=1}^{N}$ is the kth member in orthogonal sequence of K data tapers. Each taper is based on a frequency band of half-bandwidth of pf_R about a given frequency f, where $f_R = (N\Delta t)^{-1}$ is the Rayleigh frequency. Here, we choose $p = 2, K = 3$, which provides reasonable frequency resolution and sufficient spectral degrees of freedom (Mann and Park 1994, 1996). The K eigenspectras at the M grid points are organized as $M \times N$ matrix $\mathbf{A}(f)$,

$$\mathbf{A}(f) = \begin{bmatrix} w_1 Y_1^{(1)} & w_1 Y_2^{(1)} & \cdots & w_1 Y_K^{(1)} \\ w_2 Y_1^{(2)} & w_2 Y_2^{(2)} & \cdots & w_2 Y_K^{(2)} \\ \vdots & \vdots & \ddots & \vdots \\ w_M Y_1^{(M)} & w_M Y_2^{(M)} & \cdots & w_M Y_K^{(M)} \end{bmatrix}, \tag{2}$$

where the w is latitude weightings in proportion to grid point area. The matrix $\mathbf{A}(f)$ is decomposed by means of a complex SVD as

$$\mathbf{A}(f) = \sum_{k=l}^{K} \lambda_k(f)\, \boldsymbol{u}_k(f) \otimes \boldsymbol{v}_k(f) \tag{3}$$

into orthogonal modes, where λ_k represent the relative fraction of total variance explained by the kth mode, left-eigenvectors $\boldsymbol{u}_k$ represents empirical orthogonal functions in the spatial domain, and right-eigenvectors $\boldsymbol{v}_k$ represents in the spectral domain.

3. Results

3.1. Signs of recurring pattern over the recent 40 years

The recurring pattern is shown in various wildfire-related observations over California, including vegetation indices. The VHI in figure 1(b) (black line) appears to fluctuate similarly yet opposite with burned areas in figure 1(a). The trend of decline in VHI for the last 20 years is consistent with the increase of major fire damages ($r = -0.45$, since year 1987). These results describe that a drier state of vegetation provides more combustible fuel loads and a higher potential for large wildfires. Given that VHI includes greenness, it may merely reflect losses of vegetation by the wildfire occurrences rather than its flammability. However, we found consistent results from the LFM ($r = 0.67$ with VHI and -0.33 with burned area, since year 1987), which was manually collected from hundreds of sites in California to measure the water content in vegetation. As shown in figure 1(b), LFM supports that the aridity is closely associated with the danger of extreme wildfires and both variables depict a 5–7 year frequency (see the spectral analysis next). The implication from this correspondence between the burned area data and the vegetation growth factors is twofold: (a) fires tend to occur at low-moisture/drier years and (b) large fires trail high-growth years by 1–2 years with more fuel. A similar oscillating pattern also appears in three drought indices (figure 1(c)): KBDI, scPDSI and PMDI. These 'drought cycles' are in agreement with the previous indices in that more (less) vegetation grows in less (more) dry/drier years, which corresponds to the trailing enhancement (suppression) of fires, and these appear to occur in a cyclic manner.

To examine the correspondence among fire, vegetation and climate, we further conducted the cross-spectral analysis. Figure 2 shows that the cross-spectral power of VHI with all other indices of environmental conditions, including soil moisture (figure S1 (available online at stacks.iop.org/ERL/16/094031/mmedia)), reveals common periodicities that are consistently within the 5–7 year frequency band. This finding supports the inference made from figure 1 that the apparent oscillatory feature of fire intensity (burned areas) is potentially driven by a predominant intra-decadal climate oscillation. One of the prominent climate drivers of this oscillatory feature in California can be linked to the ENSO lifecycle, including its precursor and decay phase, that appears to have amplified since the late 20th century in the warming climate (Yoon *et al* 2015).

The power spectral analysis of the aforementioned variables (figures S2(a)–(d) shows a common spectral peak within the 5–7 year frequency band. The 5–7 year spectral power is significant at $p < 0.05$ among all the variables regardless of their period of record, suggesting that a 5–7 year 'climate oscillation'

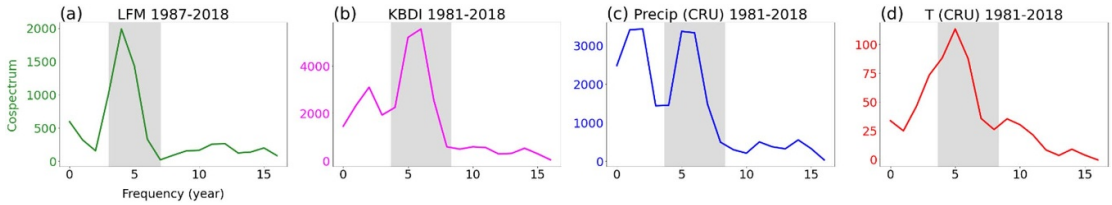

Figure 2. Cross spectrum with VHI. (a) LFM, (b) KBDI, (c) precipitation and (d) surface temperature from August 1981 to December 2018, except LFM from March 1987. The time range of 4–7 years is marked by grey. All data are considered only for California region. Linear trend is removed and 12 months moving average is applied in advance.

is a persistent feature. Among the climate factors that affect fire weather in California, precipitation exhibits a more energized 5–7 year oscillation than surface air temperature (figures S2(e) and (f)), echoing a previous observation (Los *et al* 2001) that the NDVI has a closer link with precipitation than temperature. In terms of soil moisture (figures S2(g)–(i)), the power in the 5–7 year frequency band is even more pronounced, ecohing the previous observation (Wang *et al* 2016) that the land surface processes damp atmospheric signals of higher frequencies, and the longer-term variability of precipitation remains subsequently 2015. Additional frequency analysis of the longer-term data is shown next, in section 3.2.

3.2. Validation of the frequency in the long term records

To examine whether the modern-era intra-decadal climate oscillation is similarly robust before the 21st century, we conducted the wavelet spectral analysis (Torrence and Compo 1998) for the available datasets that have longer than 100 years of record. As shown in figures 3(a) and (b), both precipitation and surface temperature show significant oscillatory characteristics in the 5–7 year frequency band throughout the 20th century. Despite their episodic occurrence, each period with an active 5–7 year oscillation in precipitation lasts around 15 years and recurs every 30 years, corresponding to the post-2000 condition. The episodes of increased 5–7 year power are even more pronounced in scPDSI in its 150 years of data (figure 3(c)), with a recurrence interval of ∼30 years.

To put the apparent oscillation into the pre-instrumental perspective, we further examined a drought proxy established from tree rings (Keen *et al* 2020) of more than 500 years, the PMDI (figure 3(d)). The wavelet spectrum of the PMDI reveals repeated occurrences of the amplified 5–7 year powers from the year 1500–2000. Nonetheless, the common significant results in the 5–7 year band suggest that the recurring wet-dry pattern is not a new phenomenon due to climate change, but rather is a part of natural variability due to a clear signal of 5–7 year power in precipitation rather than temperature (figure S3). However, climate change and human factors have apparently amplified this climate oscillation's impact on droughts (Diffenbaugh *et al* 2015) and wildfires (Williams *et al* 2019), which can be clearly seen in increasing temperature and associated fire risk (Yoon *et al* 2015, Son *et al* 2021) indicated by KBDI (figure 1(c)).

3.3. Climate forcing of the oscillation

To examine possible sources of the 5–7 year recursive fire weather conditions, the first line of analysis was conducted using regression (figures S4–S6). We find that the recurring aridity in California is associated with atmospheric-ocean coupled patterns over the subtropical North Pacific. Anomalously high SST appears in the Central North Pacific and propagates during about two-year period over the mid-latitudes adjacent to Western North America (figures S4(e) and (f)). This oceanic transport is closely matched by the track of land-approaching precipitation deficits from the Central North Pacific to California (figures S5(d)–(f)), along with anomalously high pressures in 850 hPa (figures S6(d)–(f)). These results reflect the relationship in SST forcing and atmospheric variability that induced the previous extreme droughts in California (Wang and Schubert 2014, Seager *et al* 2015).

To provide a more concise depiction of these results, we perform the MTM-SVD on major climate components on a global scale. The regression and the MTM spectral analysis are calculated between VHI in California and all other variables, while the illustration of the MTM analysis (figure 4) is focused on the 4–8 year frequency range to account for truncation. In figure 4, the amplitude and phase of the MTM coherence are visualized as the length and direction of vectors, respectively, following previous studies (Mann and Park 1994, Wang *et al* 2012). The MTM-SVD spectral coherence summarizes the lead-lag relationship as phase vectors in figure 4(a). The 0° vector indicating the north represents concurrent phase with the trough of VHI in California. The degree of angle describes phase difference with VHI, for instance, the 180° vector directing the south means the opposite phase with VHI. In the coast of California, the vectors show about 90° directing the east (a quarter-phase shift) implying warmer SST appears roughly 1.5 years earlier than the aridity in California, while the middle of the Pacific at mid-latitude is 270° (opposite phase relative to coastal California).

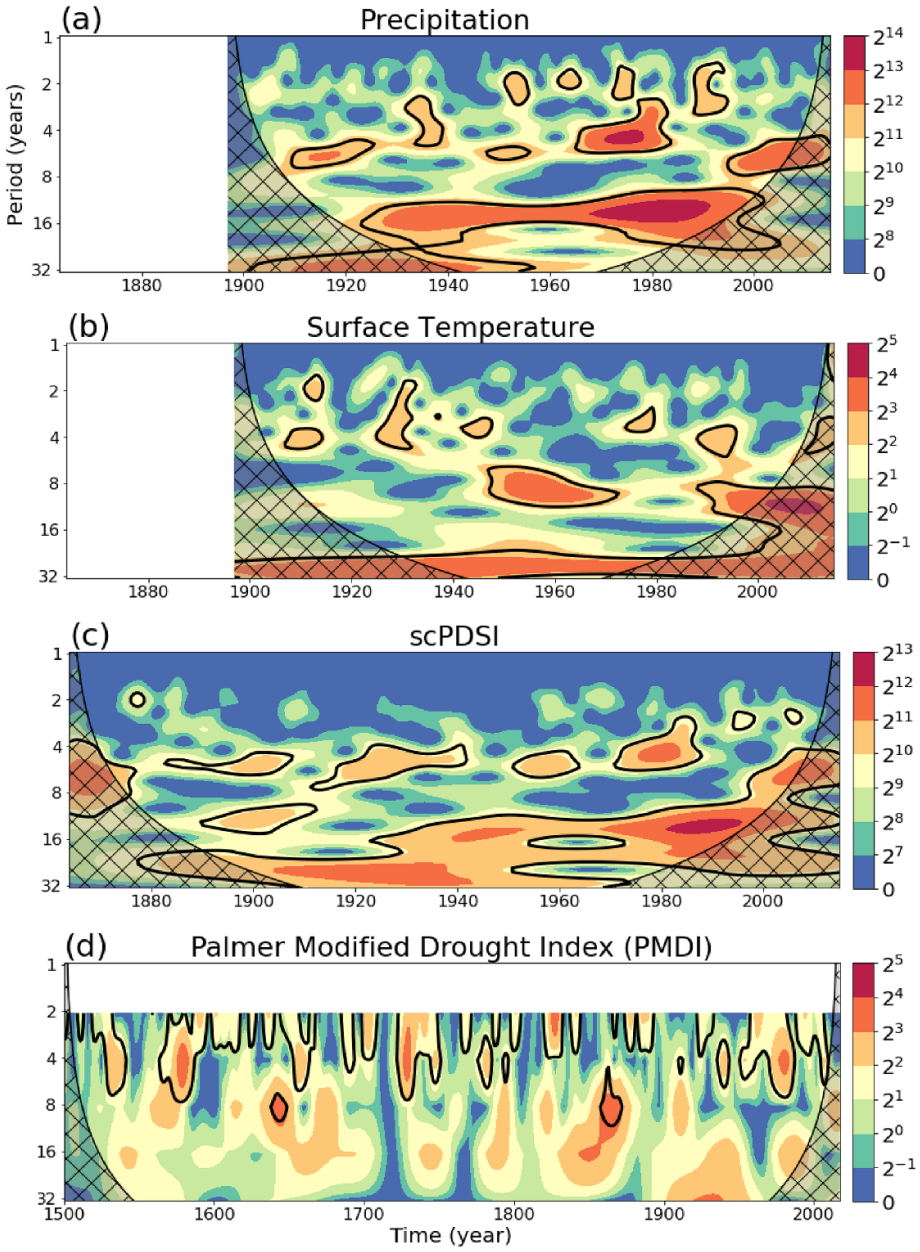

Figure 3. Wavelet spectrum. (a) precipitation, (b) surface temperature, (c) scPDSI, (d) PMDI. All data are considered only for California region. Linear trend is removed and 12 months moving average is applied in advance. Wavelet spectrum is based on Morlet parameter-6 approach and contour black line is for 95% confidence level (CI, $p < 0.05$). The red noise in 95% CI are hatched.

These two opposite phases are smoothly connected with anticlockwise rotation from the middle of the Pacific to the coast of California, accompanying a pair of negative-positive SST anomalies. These results portray that the SST anomalies propagate eastward during the few years leading up to the low VHI or drought year in California (figures S4(b) and (e)).

Similar with the SST, the precipitation shows negative anomalies in the Western North America (figure 4(b)) accompanied by a La Niña-like response in the equatorial Pacific. The developing La Niña pattern in SST and precipitation (figures S5 and S6(d)–(f)) suggests that the ENSO cycle may serve as the driver of this multi-year propagation (Wang S-Y *et al* 2015). However, the 0° vectors around California are continued rotating not only to the tropical warm pool region, but also to the North Western Pacific, which is discussed as an ENSO precursor (Wei *et al* 2016). This result, in turn, echoes the previous observation that the extreme phasing of ENSO is not the only factor responsible for the climate and vegetation variability in California (Wang *et al* 2013, Capotondi *et al* 2019).

In terms of the atmospheric teleconnection, we observe a consistent variation in the 850 hPa geopotential height regression, which shows a significantly amplified pattern (figure 4(c)) representing the North American dipole with a broadened ridge in the west and a deepened trough in the east (Wang *et al* 2015

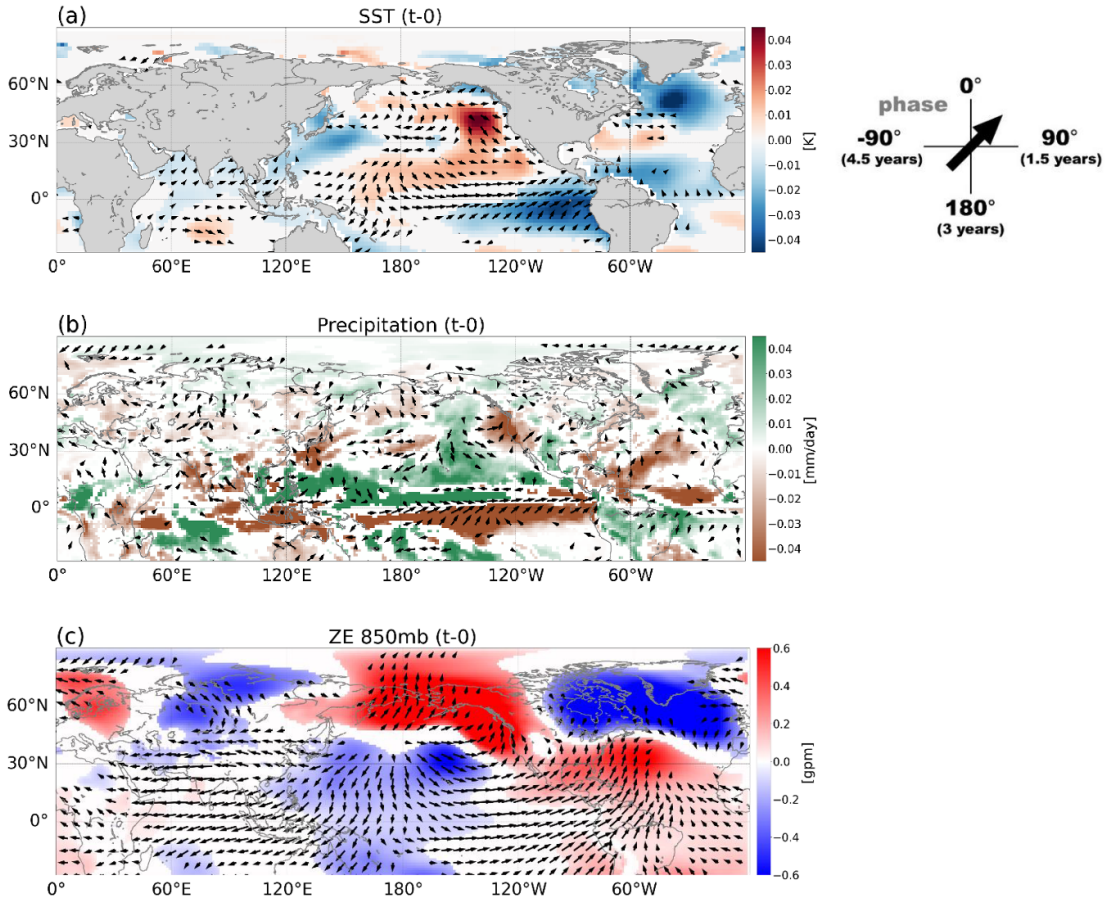

Figure 4. Regression and MTM-SVD spectral coherence based on VHI in California. Regression (shading) and maximum coherence (vector, amplitude is for length and phase is for direction) between VHI in California and anomalies of (a) SST, (b) precipitation, (c) geopotential height 850mb (zonal mean is removed). Only statistically significant ($p < 0.01$) regression and coherences are visualized. Linear trend is removed and 12 months moving average is applied in advance.

and Singh *et al* 2016). The spectral coherence displays 180° shifts of phase between California (directing north) and the north central Pacific (directing south), suggesting a wave train across the North Pacific (figures S6(b) and (e)). Two years prior to the lowest VHI, the geopotential height pattern reaching western North America (figure S6(e)) resembles the Pacific North American (PNA) (Renwick and Wallace 1996) that is known to be associated with California's drought (Lin *et al* 2017) and wildfire (Trouet *et al* 2009) . The noticeable tropical phase vectors pointing 180° away in between the Dateline (270° to the west and 90° to the east) suggest an ENSO pattern about two years before the driest state of vegetation in California.

3.4. Putting all together

To examine California's VHI connection with prominent climate modes, we provide the correlation matrix in figure S7. VHI has the correlation coefficients of above 0.3 with all ENSO-related indices, such as Niño 4 of the previous year, the Pacific Meridional Mode (PMM) SST index (Chiang and Vimont 2004) and the Trans-Niño Index (Trenberth and Stepaniak 2000) without lead (figures S7(a)–(c)). We additionally compare other known atmosphere-based indices, which have significant climatological effects in North America, including the North Atlantic Oscillation (NAO) and 'ridge-trough dipole index'(Wang *et al* 2014) (figures S7(d)–(f)). Among them, the PNA shows the highest correlation (0.4), three months prior to the vegetation peak in California. It has been known that the positive PNA in winter leads to a warmer climate in California, a decline of the snowpack and less soil moisture in the summer, resulting in more aridity and wildfire risks (Abatzoglou 2011). However, our results are contradictory, showing a significant positive correlation (0.56, $p < 0.01$) between spring PNA and summer VHI (table S1). When the spring PNA is regressed on the geopotential height in 850mb, the positive phase of PNA pattern appears on the atmosphere (figure S8(a)). The ocean reflects El Niño pattern in the previous summer in relation to the spring PNA (figure S8(b)), being more pronounced through the comparison of the time-series of Niño 4 and time lagged PNA (figure S9). Considering these results, even though there have been arguments that ENSO and PNA

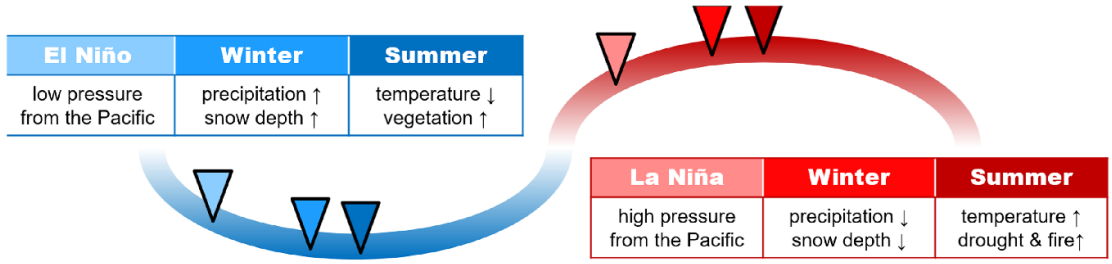

Figure 5. Diagram of the teleconnection hypothesis for hydrological oscillation in California. The lower/upper bound of wildfire risk in California is divided into blue/red. The premature state (∼2 years before) for each phase is represented by light blue/red, the early warning state (3∼6 months before) is by blue/red and the peak state is by dark blue/red. Each progress is marked with a colored inverted triangle on the cycle line and climatological features are summarized on the tables.

are independent of each other (Straus and Shukla 2002), we infer that the positive PNA pattern in spring, which plays a role of precursor of vigorous stage of vegetation in California summer, is associated with ENSO dynamics. Table S1 summaries statistically significant relationship with time differences between ENSO related atmospheric-ocean circulation and hydrological components, such as precipitation and snowpack. Only the spring PNA and the snow depth, however, are not significantly correlated. This is probably obvious because high pressure is enhanced over the western US in the positive PNA phase, inducing warmer and drier state in California (Ault *et al* 2011). Instead, the negative phase of NAO, which is shown in figure S7(e), is known for the spring snowmelt to be delayed in the negative NAO phase (Myoung *et al* 2015, 2017). A combination with the North Pacific Oscillation is also suggested to explain the drought process in California (Lin *et al* 2017).

Even though there is no consensus yet on what climate modes govern the variability of vegetation phenology in California, several combinations between oceanic and atmospheric oscillations are suggested for the better depiction of the climate variability (Lin *et al* 2017, Liu *et al* 2018). In our study, the results of the MTM-SVD showed that all the variables have similar phase differences with roughly 180° rotation from the common starting point in the tropical warm pool to California and to the Peruvian coast (figure 4). Also, the pattern of the eastward propagating wave train originated from the western Pacific (figure S6(b)) is also of interest and deserves further exploration. Based on these results, we assume that the PNA-associated patterns occurring in the mid-latitude may share the same source with the full lifecycle of ENSO, which with emphasis in the western Pacific, which has been suggested as a trigger for the PNA (Straus and Shukla 2002, Soulard *et al* 2019).

4. Conclusions

Wildfire has been one of the major natural disasters damaging California. Unusually large wildfires in the early wildfire season with the driest winter has raised concerns on this year's fire season. In recent years, the episodic catastrophes lead us to detect the 5–7 year frequency in agreement with multiple fire-related climate and vegetation components. Furthermore, this frequency is attested with several long-term records of more than 100 years, proving that they are not a coincidence, nor will they stop occurring in the future. We have shown a potential linkage between the frequency and teleconnections, such as ENSO and PNA. The ENSO pattern and its lifecycle are divided into two types: zonal and meridional modes. The meridional mode has a greater influence on the growth stage of El Niño (Di Lorenzo *et al* 2015). The PMM, which is more likely to trigger the Central Pacific type of ENSO, forms positive SST anomalies in the central-eastern North Pacific, 1.5 years prior to the maturing of La Niña. The similarities between the contrasting SST pair with a two-year lead (figure S4(e)) and the meridional mode strongly suggest a connection with the developing phase of ENSO and California's vegetation growth, i.e. one that includes the transition or precursor of ENSO.

Figure 5 summarizes the time flow for the 5–7 year oscillation of fire-related climate anomalies in California. In the early stages of La Niña (El Niño), atmospheric high (low) pressure propagates from the northern central Pacific. Once the high (low) pressure reaches the west coast, 3–6 months prior to the dry season in California, there are less (high) winter precipitation and snow. This is followed by negative (positive) PNA in the next spring. By the upcoming summer, the high (low) pressure will mark more (less) distress the vegetation with increasing (decreasing) temperature, eventually providing more (less) vulnerability hydroclimate environment to the extreme wildfires in California. The dynamical linkage of these empirically revealed processes requires further modeling studies to verify.

Data availability statement

The data that support the findings of this study are available upon reasonable request from the authors.

Acknowledgments

This research is funded by the GIST Research Institute (GRI) grant funded by the GIST in 2021 and the Korean Meteorological Agency under the grant KMI2018-07010. H Kim acknowledges Grant-in-Aid for Scientific Research (18KK0117) from Japan Society for the Promotion of Science (JSPS). Simon Wang is supported by U.S. Department of Energy, Office of Science under Award Number DE-SC0016605 and the National Science Foundation P2C2 Program under Award Number 1903721. We acknowledge the use of fire datasets from the MTBS (from www.mtbs.gov/direct-download) and climate reanalysis datasets from the ERA5 (from www.ecmwf.int/en/forecasts/datasets/reanalysis-datasets/era5), VHI from the NOAA STAR (from www.star.nesdis.noaa.gov/smcd/emb/vci/VH/vh_ftp.php), LFM from the US forest service (www.star.nesdis.noaa.gov/smcd/emb/vci/VH/vh_ftp.php), PMDI from the Living Blended Drought Atlas version2 (www.ncdc.noaa.gov/paleo-search/study/22454), CRU long term record temperature and precipitation dataset are from the University of East Anglia (https://crudata.uea.ac.uk/cru/data/hrg/), geopotential height is from JRA55 (from https://jra.kishou.go.jp/JRA-55/index_en.html), ERSSTv5 from the NCDC (www.ncdc.noaa.gov/data-access/marineocean-data/extended-reconstructed-sea-surface-temperature-ersst-v5), and soil moisture datasets are simulated by NLDAS2 from the GSFC, NASA (https://ldas.gsfc.nasa.gov/nldas/nldas-2-model-data).

ORCID iDs

Rackhun Son https://orcid.org/0000-0002-3366-495X
S-Y Simon Wang https://orcid.org/0000-0003-2009-2275
Seung Hee Kim https://orcid.org/0000-0002-5949-8996
Hyungjun Kim https://orcid.org/0000-0003-1083-8416
Jee-Hoon Jeong https://orcid.org/0000-0002-3358-3949
Jin-Ho Yoon https://orcid.org/0000-0002-4939-8078

References

Abatzoglou J T 2011 Influence of the PNA on declining mountain snowpack in the Western United States *Int. J. Climatol.* **31** 1135–42

Abatzoglou J T, Williams A P and Barbero R 2019 Global emergence of anthropogenic climate change in fire weather indices *Geophys. Res. Lett.* **46** 326–36

Ault T R, Macalady A K, Pederson G T, Betancourt J L and Schwartz M D 2011 Northern Hemisphere modes of variability and the timing of spring in western North America *J. Clim.* **24** 4003–14

Capotondi A, Sardeshmukh P D, Di Lorenzo E, Subramanian A C and Miller A J 2019 Predictability of US West Coast Ocean Temperatures is not solely due to ENSO *Sci. Rep.* **9** 1–10

Chen F, Mitchell K, Schaake J, Xue Y, Pan H L, Koren V, Duan Q Y, Ek M and Betts A 1996 Modeling of land surface evaporation by four schemes and comparison with FIFE observations *J. Geophys. Res. Atmos.* **101** 7251–68

Chiang J C H and Vimont D J 2004 Analogous meridional modes of atmosphere–ocean variability in the tropical Pacific and tropical Atlantic *J. Clim.* **17** 4143–58

Cook E R, Seager R, Heim R R, Vose R S, Herweijer C and Woodhouse C 2010 Megadroughts in North America: placing IPCC projections of hydroclimatic change in a long-term palaeoclimate context *J. Quat. Sci.* **25** 48–61

Dai A, Trenberth K E and Qian T 2004 A global dataset of Palmer Drought Severity Index for 1870–2002: relationship with soil moisture and effects of surface warming *J. Hydrometeorol.* **5** 1117–30

Di Lorenzo E, Liguori G, Schneider N, Furtado J C, Anderson B T and Alexander M A 2015 ENSO and meridional modes: a null hypothesis for Pacific climate variability *Geophys. Res. Lett.* **42** 9440–8

Diffenbaugh N S, Swain D L, Touma D and Lubchenco J 2015 Anthropogenic warming has increased drought risk in California *Proc. Natl Acad. Sci. USA* **112** 3931–6

Dimitrakopoulos A P and Papaioannou K K 2001 Flammability assessment of Mediterranean forest fuels *Fire Technol.* **37** 143–52

Harris I, Osborn T J, Jones P and Lister D 2020 Version 4 of the CRU TS monthly high-resolution gridded multivariate climate dataset *Sci. Data* **7** 1–18

Heddinghaus T R and Sabol P 1991 A review of the Palmer Drought Severity Index and where do we go from here *Proc. 7th Conf. on Applied Climatology* (Citeseer) pp 242–6

Hersbach H *et al* 2020 The ERA5 global reanalysis *Q. J. R. Meteorol. Soc.* **146** 1999–2049

Huang B, Thorne P W, Banzon V F, Boyer T, Chepurin G, Lawrimore J H, Menne M J, Smith T M, Vose R S and Zhang H M 2017 Extended reconstructed Sea surface temperature, Version 5 (ERSSTv5): upgrades, validations, and intercomparisons *J. Clim.* **30** 8179–205

Jolly W M, Cochrane M A, Freeborn P H, Holden Z A, Brown T J, Williamson G J and Bowman D M J S 2015 Climate-induced variations in global wildfire danger from 1979 to 2013 *Nat. Commun.* **6** 7537

Karl T R 1986 The sensitivity of the Palmer Drought Severity Index and Palmer's Z-index to their calibration coefficients including potential evapotranspiration *J. Clim. Appl. Meteorol.* **25** 77–86

Keeling C D, Whorf T P, Wahlen M and Van Der Plichtt J 1995 Interannual extremes in the rate of rise of atmospheric carbon dioxide since 1980 *Nature* **375** 666–70

Keen R M, Voelker S L, Bentz B J, Wang S-Y S and Ferrell R 2020 Stronger influence of growth rate than severity of drought stress on mortality of large ponderosa pines during the 2012–2015 California drought *Oecologia* **194** 359–70

Keetch J J and Byram G M 1968 *A Drought Index for Forest Fire Control* vol 38 (US Department of Agriculture, Forest Service, Southeastern Forest Experiment)

Kobayashi S *et al* 2015 The JRA-55 reanalysis: general specifications and basic characteristics *J. Meteorol. Soc. Japan* **93** 5–48

Kogan F N 1995 Application of vegetation index and brightness temperature for drought detection *Adv. Space Res.* **15** 91–100

Koster R D and Suarez M J 1992 Modeling the land surface boundary in climate models as a composite of independent vegetation stands *J. Geophys. Res.* **97** 2697–715

Liang X, Lettenmaier D P, Wood E F and Burges S J 1994 A simple hydrologically based model of land surface water and energy fluxes for general circulation models *J. Geophys. Res.* **99** 14415–28

Lin Y-H, Hipps L E, Wang S-Y S and Yoon J-H 2017 Empirical and modeling analyses of the circulation influences on California precipitation deficits *Atmos. Sci. Lett.* **18** 19–28

Liu Y C, Di P, Chen S H and DaMassa J 2018 Relationships of rainy season precipitation and temperature to climate indices in California: long-Term variability and extreme events *J. Clim.* **31** 1921–42

Liu Y, Stanturf J and Goodrick S 2010 Trends in global wildfire potential in a changing climate *For. Ecol. Manage.* **259** 685–97

Los S O, Collatz G J, Bounoua L and Tucker C J 2001 *535 Global Interannual Variations in Sea Surface Temperature and Land Surface Vegetation, Air Temperature, and Precipitation* vol 14 (American Meteorological Society) pp 1535–49

Mann M E and Lees J M 1996 Robust estimation of background noise and signal detection in climatic time series *Clim. Change* **33** 409–45

Mann M E and Park J 1994 Global-scale modes of surface temperature variability on interannual to century timescales *J. Geophys. Res.* **99** 25819–33

Mann M E and Park J 1996 *Joint Spatiotemporal Modes of Surface Temperature and Sea Level Pressure Variability in the Northern Hemisphere during the Last Century* vol 9 (American Meteorological Society) pp 2137–62

McLauchlan K K, Higuera P E, Miesel J, Rogers B M, Schweitzer J, Shuman J K, Tepley A J, Varner J M, Veblen T T and Adalsteinsson S A 2020 Fire as a fundamental ecological process: research advances and frontiers *J. Ecol.* **108** 2047–69

Myoung B, Kim S H, Kim J and Kafatos M C 2015 On the relationship between the North Atlantic Oscillation and early warm season temperatures in the southwestern United States *J. Clim.* **28** 5683–98

Myoung B, Kim S H, Kim J and Kafatos M C 2017 On the relationship between spring NAO and snowmelt in the upper southwestern United States *J. Clim.* **30** 5141–9

Palmer W C 1965 *Meteorological Drought* vol 30 (US Department of Commerce, Weather Bureau)

Park J, Lindberg C R and Vernon F L 1987 Multitaper spectral analysis of high-frequency seismograms *J. Geophys. Res.* **92** 12675

Pollet J and Brown A 2007 Fuel moisture sampling guide (*Bur. L. Manag. Utah State Off. Salt Lake City, UT, USA* (available at: https//www.wfas.net/nfmd/references/fmg.pdf) (Accessed 10 March 2017)

Rajagopalan B and Lall U 1998 Interannual variability in western US precipitation *J. Hydrol.* **210** 51–67

Renwick J A and Wallace J M 1996 *Relationships between North Pacific Wintertime Blocking, El Niño, and the PNA Pattern* vol 124 (American Meteorological Society) p 2071–76

Rogers B M, Soja A J, Goulden M L and Randerson J T 2015 Influence of tree species on continental differences in boreal fires and climate feedbacks *Nat. Geosci.* **8** 228–34

Seager R, Hoerling M, Schubert S, Wang H, Lyon B, Kumar A, Nakamura J and Henderson N 2015 Causes of the 2011–14 California drought *J. Clim.* **28** 6997–7024

Simon Wang S-Y, Lin Y-H, Gillies R R and Hakala K 2016 Indications for protracted groundwater depletion after drought over the Central Valley of California *J. Hydrometeorol.* **17** 947–55

Singh D, Swain D L, Mankin J S, Horton D E, Thomas L N, Rajaratnam B and Diffenbaugh N S 2016 Recent amplification of the North American winter temperature dipole *J. Geophys. Res. Atmos.* **121** 9911–28

Son R, Kim H, Wang S-Y S, Jeong J-H, Woo S-H, Jeong J-Y, Lee B-D, Kim S H, LaPlante M and Kwon C-G 2021 Changes in fire weather climatology under 1.5 °C and 2.0 °C warming *Environ. Res. Lett.* **16** 034058

Soulard N, Lin H and Yu B 2019 The changing relationship between ENSO and its extratropical response patterns *Sci. Rep.* **9** 1–10

Straus D M and Shukla J 2002 *Does ENSO Force the PNA?* vol 15 (American Meteorological Society) p 2340–58

Thomson D J 1982 Spectrum Estimation and Harmonic Analysis *Proc. IEEE* **70** 1055–96

Torrence C and Compo G P 1998 *A Practical Guide to Wavelet Analysis* vol 79 (American Meteorological Society) pp 61–78

Trenberth K E and Stepaniak D P 2000 *LETTERS Indices of El Niñ O Evolution* vol 14 (American Meteorological Society)

Trouet V, Taylor A H, Carleton A M and Skinner C N 2009 Interannual variations in fire weather, fire extent, and synoptic-scale circulation patterns in northern California and Oregon *Theor. Appl. Climatol.* **95** 349–60

Wang H and Schubert S 2014 Causes of the extreme dry conditions over California during early 2013 *Bull. Am. Meteorol. Soc.* **95** S7–S11

Wang S S, Huang W and Yoon J 2015 The North American winter 'dipole' and extremes activity: a CMIP5 assessment *Atmos. Sci. Lett.* **16** 338–45

Wang S Y, Gillies R R and Reichler T 2012 Multidecadal drought cycles in the great basin recorded by the Great Salt Lake: modulation from a transition-phase teleconnection *J. Clim.* **25** 1711–21

Wang S-Y S, Jiang X and Fosu B 2015 Global eastward propagation signals associated with the 4–5-year ENSO cycle *Clim. Dyn.* **44** 2825–37

Wang S-Y, L'Heureux M and Yoon J-H 2013 Are greenhouse gases changing ENSO precursors in the western North Pacific? *J. Clim.* **26** 6309–22

Wang S, Hipps L, Gillies R R and Yoon J 2014 Probable causes of the abnormal ridge accompanying the 2013–2014 California drought: ENSO precursor and anthropogenic warming footprint *Geophys. Res. Lett.* **41** 3220–6

Wei J, Jin Q, Yang Z-L and Dirmeyer P A 2016 Role of ocean evaporation in California droughts and floods *Geophys. Res. Lett.* **43** 6554–62

Wells N, Goddard S and Hayes M J 2004 *A Self-Calibrating Palmer Drought Severity Index* vol 17 (American Meteorological Society) pp 2335–51

Williams A P, Abatzoglou J T, Gershunov A, Guzman-Morales J, Bishop D A, Balch J K and Lettenmaier D P 2019 Observed impacts of anthropogenic climate change on wildfire in California *Earth's Future* **7** 892–910

Yoon J H, Wang S Y S, Gillies R R, Kravitz B, Hipps L and Rasch P J 2015 Increasing water cycle extremes in California and in relation to ENSO cycle under global warming *Nat. Commun.* **6** 1–6